Research Article

Failure Mechanism and Parameter Analysis of Outer Sleeve Joints under Reciprocating Load

Dan Zhang[*] and Lei Zhang

College of Civil Engineering, Hunan City University, Yiyang 413000, China

_____

Abstract

The beam-column joint is an important force transferring hub in a frame system whose seismic performance directly affects the overall response of the structure. To reveal the force transmission path and explore the seismic performance of joints, a numerical analysis method for a new outer sleeve joint of a square steel tubular column-H-shaped steel beam was proposed in this study. The failure modes and mechanical properties of four outer sleeve joints under reciprocating load were analyzed using the finite element software ABAQUS. On the basis of the stress distribution characteristics of components, the failure mechanism of each component of the joints was revealed, and the shear force transfer path in the joint core area was obtained. In addition, a parameter analysis was carried out from the three aspects of material parameters, geometric parameters, and load parameters, and the factors affecting the seismic performance of the joints were discussed. Results show that the failure of the plastic hinge at the beam end satisfies the design requirements of strong joint and weak member and that the geometric dimension is the key factor affecting the failure mode and seismic performance indicators of joints. The stiffener ribs bear 26.2% to 59.2% of the shear force during the shear force transfer process in the joint core area. As the distance from the joint core area decreases, the shear force assumed by the beam web is reduced. The linear stiffness ratio and the flexural capacity ratio of the beam-to-column are identified as the major parameters affecting the failure mode of outer sleeve joints, and their recommended values are 0.536 and 0.372, respectively, combined with the seismic performance of joints. This study provides an important foundation for determining the reasonable values of outer sleeve joints in steel frame design.

Keywords: Beam-column joint, Outer sleeve, Reciprocating load, Failure mechanism, Parameter analysis
_____

1. Introduction

In the design of steel structures, the joint connection makes the beam and column work together and ensures the effective transmission of loads. The performance of the joint connection directly affects the overall response of the structure, which is considered top priority in steel structure design. Rigid joints are mostly used in steel frames to ensure that the connection between beams and columns has sufficient stiffness. The joint form is mainly bolt–weld connection, which has been widely used in steel structures given its high strength and good ductility [1].

However, during the Northridge earthquake in the US and the Hyogoken–Nanbu earthquake in Japan in the 1990s, a large number of welded beam–column joints have experienced brittle fractures, and a plastic hinge was not formed at the beam end to dissipate seismic energy. In addition, the steel frame, which has always been expected to demonstrate good seismic performance, did not show the expected ductility and energy dissipation capacity, which has attracted much attention from the international engineering community.

The plastic hinge failure at the beam end meets the seismic requirements of strong joints and weak members. Therefore, to prevent the joint weld area with poor toughness from being damaged, several measures can be taken during the design to keep the position of the plastic hinge away from the welds. Scholars have examined two

main methods for measuring the outward movement of plastic hinges [2-6], namely, the local strengthening of joints and the local weakening of the beam section. Both the strengthened and weakened joints adopt either strengthening or weakening measures for steel beams to transfer the position of the plastic hinge outside the beam–column connection. However, for the square steel tubular column-H-shaped beam connection with a good seismic performance, the thickness of the column wall is a key parameter that affects the mechanical performance of the joint. In the hollow steel tube column–beam joint, the damage is mostly related to the excessive deformation of the column wall [7]. Accordingly, how to strengthen the square steel tubular column in the beam–column joint area and clarify the seismic performance of the column-wall-strengthened joints is an urgent problem that needs to be solved.

Following the above analysis, the outer sleeve was employed in this study to locally thicken the square steel tubular column wall in the joint area [8] and to enhance the stiffness and prevent the local buckling of the joint. By establishing a finite element model and conducting parameter analysis, the seismic performance and influencing parameters of the outer sleeve joints under reciprocating load were analyzed with an aim to reveal the failure mechanism and force transmission path of the joints from a microscopic perspective and to provide references for the design of outer sleeve joints.

_____

2. State of the art

The beam–column connection welds of the steel frame are prone to brittle fractures in case of earthquakes and are thereby considered weak links in joint design. Therefore, stiffening members are usually employed to transfer loads of the square steel tubular column-H-shaped steel beam joint and to move the position of the plastic hinge outside the beam–column connection. In this way, the risk of brittle failure of welds is reduced, and the main reinforcing forms include the stiffening connection and cover plate connection. Liu et al. [9] studied the seismic performance of the bolted stiffened endplate joints of H-section steel beams to square hollow structural steel (HSS) columns by conducting tests and adopting finite element methods. They found that the proposed bolted connection shows good hysteresis behavior and ductility. However, almost all specimens showed deformation at the endplate of the stiffening position, and only one specimen exhibited plastic hinge at the beam end outside the cover plate. Wang et al. [10] and Roudsari et al. [11] used penetrated gusset plates and stiffened channel links, respectively, to strengthen concrete-filled steel tube (CFST) column–beam joints. They found that setting penetrated gusset plates and stiffened channel links can move the plastic hinge of the beam end away from the column wall, but the brittle cracking of the welds cannot be avoided at the end of loading. By taking the combined effect of steel tube and concrete into account, Zhu et al. [2] conducted tensile experiments on CFST exterior-diaphragm stiffened connections and found that the longitudinal stiffener alleviates the deformation concentration in the joint area. However, they did not examine whether the joint formed a plastic hinge under reciprocating load. For cover plate connection joints, Wang et al. [3] proposed a design method for steel frame connections with low yield point steel ductile fuses and discussed the quantitative relationship between different influencing factors and the action of the cover plate structural fuse. However, the factors affecting the low yield point steel cover plate cannot be ignored as they can increase the difficulty of implementing the design. Zhang et al. [12] used flange cover plates to improve the seismic performance of prefabricated joints, but the failure mode of these joints is largely affected by multiple parameters, such as cover plate thickness, material properties, and the gap between beams. For the square HSS column to H-section beam connections with double cover plates, Zhan et al. [13] found that the joint dissipates energy by sliding the contact surface of the cover plates and the plastic deformation of the bolt holes, which would pinch the hysteretic curves. The knee brace was also identified as an effective measure for improving the seismic capacity of the joint area. Cho et al. [4] studied the mechanical properties of modular steel joints with four knee braces and found that setting knee braces improved the bearing capacity and stiffness of beam–column joints. However, the effects of these joints on the deformation of spliced beam members were inconsistent.

Strengthening members can make the bearing capacity of the joints larger than that of the components. Dialectically, the flexural bearing capacity of the beam ends can be weakened to make the bearing capacity of the joints larger than that of the components, the most typical of which are the reduced beam section (RBS) joints. To improve the potential brittle failure of RBS rigid joints, Heidari et al. [14] designed proper holes and notches on the beam flange. However, the beam flange between the drilled holes was torn in the process. Parvari et al. [15] evaluated the seismic performance of moment-resisting connections with drilled flange beams and found that the presence of holes increases in rotation during the maximum moment. By comparing the mechanical properties of non-drilled beam flange, reduced beam section, drilled flange connection, and drilled connection with a variable diameter corresponding to the diamond-shaped hole, Vajdian et al. [16] found that those variable diameter drilling joints related to diamond holes demonstrate a better behavior and that opening the diamond-shaped holes increases the difficulty of component production. To improve the hysteretic performance of RBS joints, Roudsari et al. [17] conducted a large number of nonlinear finite element analyses (FEA) on RBS joints with radius cut, straight cut, and drilled flanges, but their findings did not propose suggested values for each influencing parameter. The reduced web section (RWS) can also achieve the purpose of weakening the beam section. Yu et al. [5] studied steel frames with RWS connections and found that RWS sections improve the seismic collapse resistance of a structure and that the frame with RWS connections sacrifices structural safety at non-collapse stages. Kolbadi et al. [18] introduced a slotted web connection that reduces the plastic strain equivalent to the panel zone. However, the slotted web and bolted flange weaken the section to a certain extent. Imanpour et al. [19] and Jiang et al. [20] suggested using corrugated webs to replace some or all flat webs within an area near the joints, which would reduce the beam flexural strength and force the plastic hinge to form in the corrugated zone. However, they ignored the influence of detailed waveform parameters on the performance of joints.

The above studies focus on the seismic performance of stiffening and RBS joints of square steel tubular column-H-shaped steel beams. Although the expected plastic hinge failure mode was obtained, the beam–column connection is complex, the force transmission path is not clear, and the weakened beam section with a large internal force negatively affects the seismic performance of the structure. Therefore, the connection method and seismic performance of the square steel tubular column-H-shaped steel beam joints need to be further studied. This study proposes a new type of square steel tube column-H-shaped steel beam outer sleeve joint with a clear internal force transmission path, high degree of prefabrication, and easy installation. A 3D FEA model was also built using ABAQUS to investigate the failure mode and seismic performance of the joints. By analyzing the stress distribution of the joints and components accurately, the stress process and force transfer mechanism were revealed. Starting from the material, geometric, and load parameters, the failure mode and moment–rotation relationship of the outer sleeve joints were discussed. The main parameters affecting the seismic performance of the joints were determined, and suggestions for the design of outer sleeve joints were proposed.

The rest of this study is organized as follows. Section 3 introduces the finite element modeling method and verification. Section 4 reveals the failure mechanism and shear transfer path of outer sleeve joints through the stress distribution of joints and components and discusses the influence laws of different parameters on the performance of outer sleeve joints via parameter analysis. Section 5 presents the conclusions.

3. Methodology

Using the finite element method, the 3D analysis model of outer sleeve joints was established. The geometric parameters, material constitutive relationship, meshing method and loading system, and accuracy of this model were then verified.

3.1 Finite element model of outer sleeve joints
The finite element software ABAQUS [21] was used to simulate and analyze four cross-shaped full-scale joints. The specimens were divided into groups A and B according to the different cross-sectional dimensions of their beams and columns. Each group contained a hollow steel tube joint (HSTJ) and a concrete-filled steel tube joint (CFSTJ). The height of the square steel tube column was 3000 mm, and the lengths of the H-shaped steel beam for groups A and B were 2000 mm and 3000 mm, respectively. The joint configuration is shown in Fig. 1, whereas the detailed parameters are shown in Table 1. The beam and column

were connected by T-stubs using high-strength bolts. The T-stub was provided with a stiffener rib. The flange and web of the T-stub were connected by four and six high-strength bolts, respectively. High-strength bolts of 10.9 grade were selected.

3.2 Material constitutive relation
The joint model was made of Q345 steel. According to the test results for the previous material property [8], the stress–strain curves of the square steel tubular column, H-shaped steel beam, T-stub, and other components were obtained, and the bilinear analysis models were established. In addition, the concrete constitutive model considering the confinement of steel tube was employed to simulate the stress–strain relationship of the core concrete [22]. The anti-slip coefficient of the contact surfaces was set to 0.5, and the pretension forces of M16 and M20 high-strength bolts were set to 100 kN and 155 kN, respectively.

Table 1. Parameters of the outer sleeve joint specimens

Specimens	Steel tubular column	H-shaped steel beam	Axial compression ratio	T-stub		Outer sleeve	
				Web	Flange	Beam side	Beamless side
A-HSTJ	300×300×8	H248×124×5×8	0.3	300×200×11	200×200×17	496×300×12	496×300×8
A-CFSTJ	300×300×8	H248×124×5×8	0.3	300×200×11	200×200×17	496×300×12	496×300×8
B-HSTJ	350×350×8	H346×174×6×9	0.3	300×260×11	260×200×17	692×350×16	692×350×8
B-CFSTJ	350×350×8	H346×174×6×9	0.3	300×260×11	260×200×17	692×350×16	692×350×8
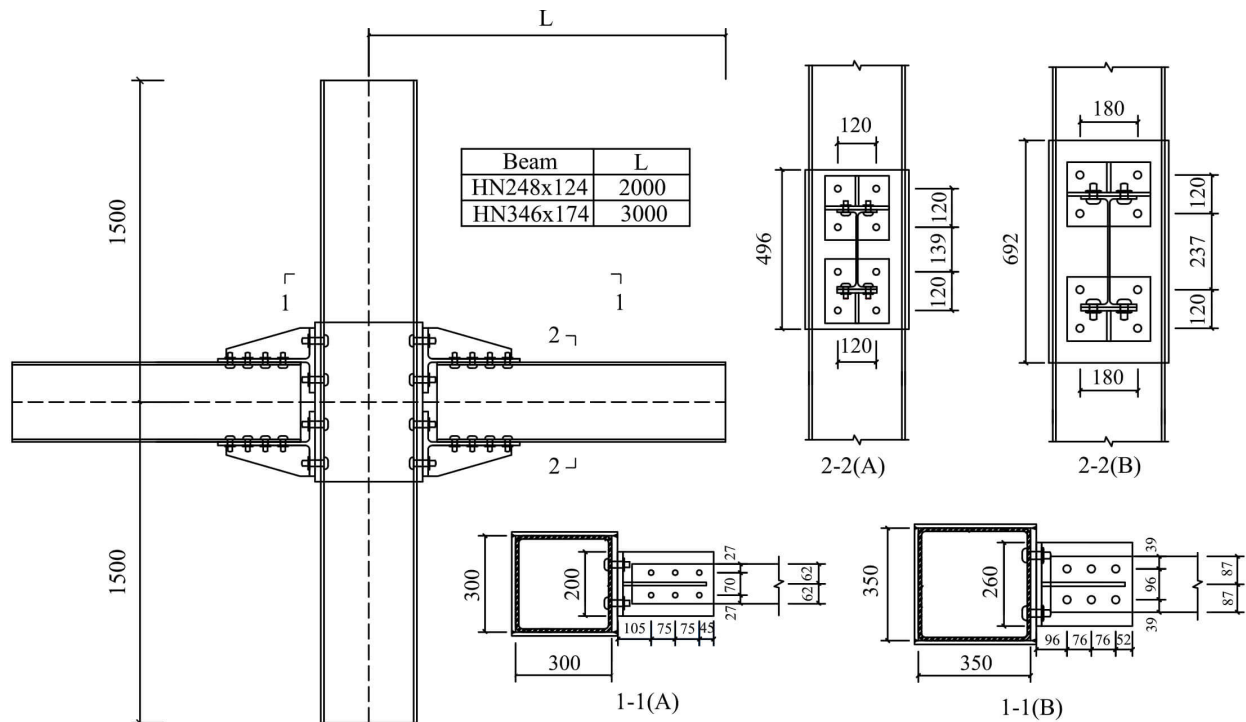
Fig. 1. Model dimensions of outer sleeve joints (units: mm)

3.3 Material constitutive relation
The 3D solid elements C3D8R combined with structured adaptive mesh generation were used to mesh the joints. Given the complex stress in the joint area, the mesh subdivision of the core area and beam end warrants further exploration, whereas the mesh division located far away from the joint area can be relatively sparse. Coulomb friction was adopted to describe the contact surfaces between the H-shaped steel beam and T-stub web, between the outer sleeve and T-stub flange, and between the nut and T-stub. The contact between the screw and bolt hole was defined as hard contact. The welding relationships among the components,

such as from the outer sleeve to the column wall and from the stiffening rib to the T-stub, were imitated by tie contact.

To accurately reflect the boundary conditions in testing the square steel tube column-H-shaped steel beam joint, the anti-symmetric reciprocating loading method was applied at the beam end. The loading process was divided into three steps. First, the specified pre-tightening force was applied to the high-strength bolts. Second, the uniform vertical force was applied on top of the column according to a 0.3 axial compression ratio. Third, the anti-symmetric reciprocating force was simultaneously added to the left and right free

ends of the beam to obtain the force–displacement curves. The reciprocating loading system is shown in Fig. 2.
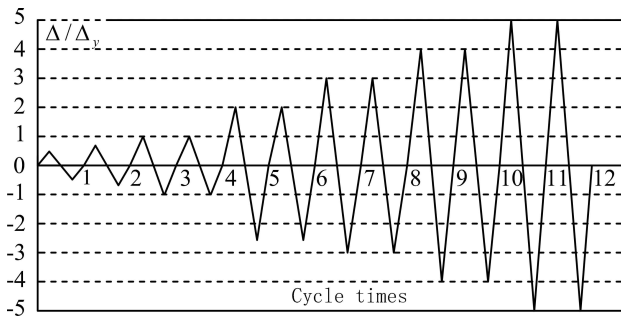
Fig. 2. The reciprocating loading system

3.4 Verification of the finite element model
The accuracy of the finite element model was preliminarily verified in previous studies. Fig. 3 shows the failure modes of outer sleeve joints obtained via experiments and numerical simulation. The beam-end plastic hinge of the A group of specimens was damaged, whereas the T-stub web of the B group of specimens was broken, thereby indicating that the joint size has a great influence on the failure mode of the specimen. The skeleton curves obtained from the FEA and tests are shown in Fig. 4, and the FEA results were consistent with those of the tests. The flexural capacity and initial stiffness improved along with the dimension of the joints, whereas the ductility was relatively poor. The rotational stiffness of steel tubular joints was effectively improved by pouring concrete into the steel tubular columns, but the bearing capacity did not increase significantly. The following sections describe the further stress analysis, load transmission path, and parameter analysis of joints and components.

Fig. 3. Comparison of failure modes of outer sleeve joints. (a) Plastic hinge of the beam flange of the group A specimens. (b) Fracture of the T-stub flange of the group B specimens
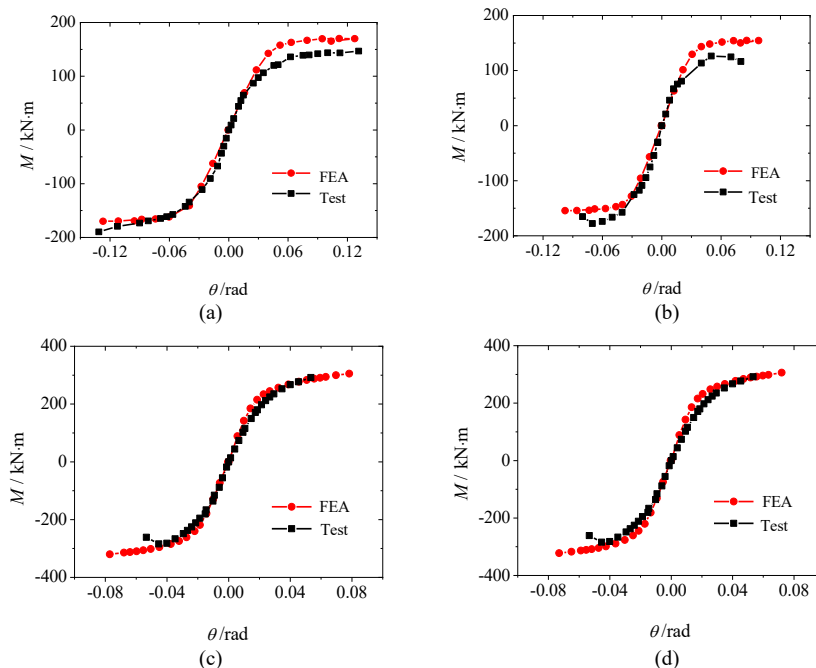
Fig. 4. Comparison analysis of skeleton curves [8]. (a) A-HSTJ. (b) A-CFSTJ. (c) B-HSTJ. (d) B-CFSTJ

4 Result Analysis and Discussion

4.1 Stress distribution of the outer sleeve joints
Using the abovementioned FEA method, further stress analysis was carried out on the outer sleeve joints and components, that is, the microscopic stress distribution and failure mechanism were studied. Fig. 5 shows the Mises stress of the outer sleeve joints of groups A and B specimens in the loading limit state. The stress and deformation of the group A joints are concentrated in the plastic hinge area of the beam flange. Meanwhile, the deformation and energy dissipation of the group B joints are concentrated in the T-stub, and the beam flange is not deformed. The concrete of the square steel tubular column reduces the stress in the joint area, which plays an important role in improving the mechanical properties of the structure.

4.1.1 Stress distribution of the square steel tubular column

Fig. 6(a) shows that the stress of the steel tubular column restrained by the outer sleeves is small under the action of axial pressure. Under a reciprocating load, the tensile and compressive stresses of the steel tubular column wall near the upper and lower T-stubs are relatively large, the deformation shows an anti-symmetric distribution, and the steel tube web has an obvious shear stress flow as shown in Fig. 6(b). The concrete can effectively reduce the stress distribution range in the core area of the joints as shown in Fig. 6(c). Larger stress values appear at the corners of the

steel tube, which are related to the cross-sectional shape and the prying force generated by the pulling force of the T-stubs.

When plastic hinges appear at the beam end of the group A specimens, the steel tube column wall reaches the yield strength, whereas the CFST column wall is still at the elastic stage, which meets the design requirements of strong columns and weak beams. As for the group B joints, the steel tube column wall connected to the T-stub reaches the yield strength as shown in Fig. 6(d). Given that the deformation of group B specimens is concentrated in the core area of the joints, the column wall deformation of these specimens is significantly larger than that of group A specimens.
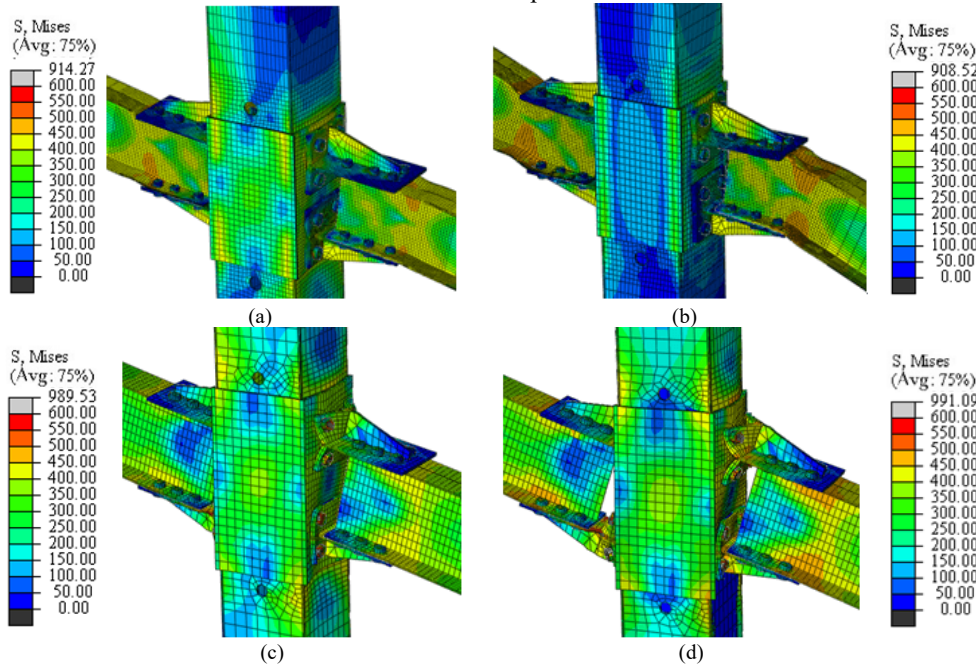
Fig. 5. Stress distribution in the core area of the outer sleeve joint specimens. (a) A-HSTJ. (b) A-CFSTJ. (c) B-HSTJ. (d) B-CFSTJ

4.1.2 Stress distribution of the outer sleeve

As shown in Fig. 7, the stress of the outer sleeves on the beam side is distributed with 1/2 of the height as the axis of symmetry. The stress values in the middle height are relatively small. The deformation is concentrated within the plastic hinge lines formed by the bolts and on both ends of the outer sleeve height. The maximum tensile stress is located at the first row of bolt holes of the outer sleeve. The stress values in the compression area are relatively small, and the maximum compressive stress appears at the edge of the outer sleeve.

When the joints are close to failure, the maximum stress of the outer sleeves of the HSTJ specimens reaches the yield strength. By taking the restraint effect of concrete into account, the stress value and distribution range of the outer sleeves of CFSTJ specimens are significantly reduced. The outer sleeves are still at the elastic stage.

4.1.3 Stress distribution of the H-shaped steel beam

The stress distribution of each group of H-shaped steel beams when loaded to the maximum value is shown in Fig. 8. The stress diagram shows a large beam flange stress at the end of the T-stub web. The maximum stress values are located at the outermost bolt holes of the beam flange. With increasing plasticity, the effective cross-sectional area of the beam flange continues to decrease, thereby resulting in the buckling of group A specimens and the emergence of plastic hinges that meet the design requirements of strong joints and

weak members. However, the stress of group B specimens is concentrated in the T-stub components. Although the beam flange reaches the yield strength locally, the deformation is small.

4.1.4 Stress distribution of the T-stub

As shown in Fig. 9, the flanges of the T-stubs in the tensile zone of groups A and B specimens tend to pull away from the column wall. Meanwhile, for the group B specimens with a large deformation in the joint core area, the deformation of the T-stub is highly significant. The junction of the flange and the web of the T-stub have large edge stress values and reach the yield at the earliest.

4.1.5 Stress distribution of the high-strength bolts

Fig. 10 shows that the maximum stress of the high-strength bolts of the column wall in the tensile area almost reaches yield strength due to the serious deformation of the T-stub flange of group B specimens. A reciprocating extrusion is observed between the nuts and holes, and the maximum stress is observed at the junction of the screws and nuts. While the buckling failure of the beam flange is observed in group A specimens, the high-strength bolts of the column wall has a small stress. Given the absence of any obvious slip at the connection position between the T-stub web and the beam flange, the high-strength bolts of the beam flange do not show a significant shear deformation, and most of them are at the elastic stage as shown in Fig. 11.
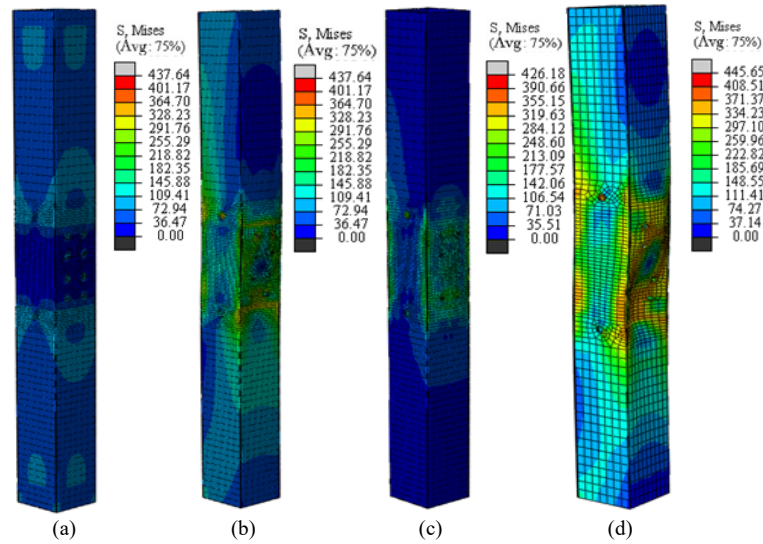
Fig. 6. Stress distribution of the square steel tubular column. (a) A-HSTJ. (b) A-CFSTJ. (c) B-HSTJ. (d) B-CFSTJ
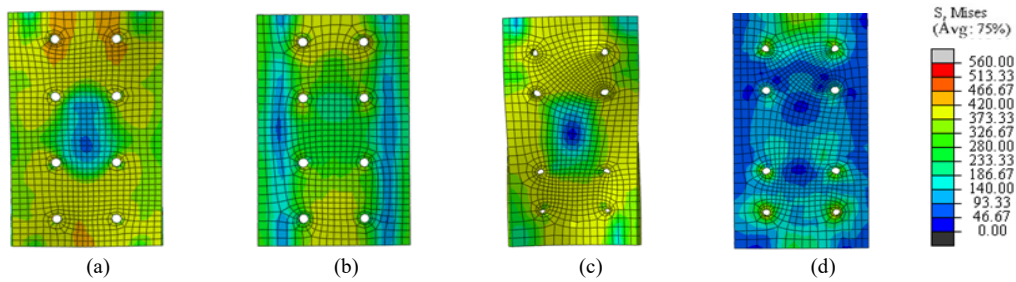
Fig. 7. Stress distribution of the outer sleeve. (a) A-HSTJ. (b) A-CFSTJ. (c) B-HSTJ. (d) B-CFSTJ
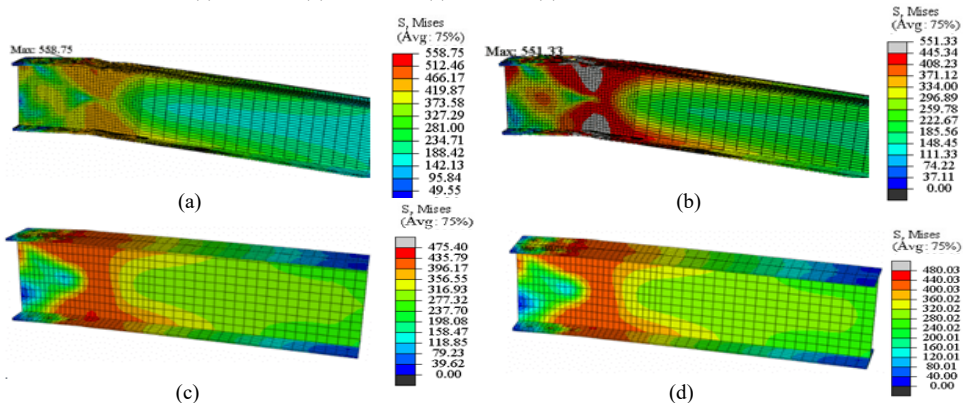
Fig. 8. Stress distribution of H-shaped steel beam. (a) A-HSTJ. (b) A-CFSTJ. (c) B-HSTJ. (d) B-CFSTJ
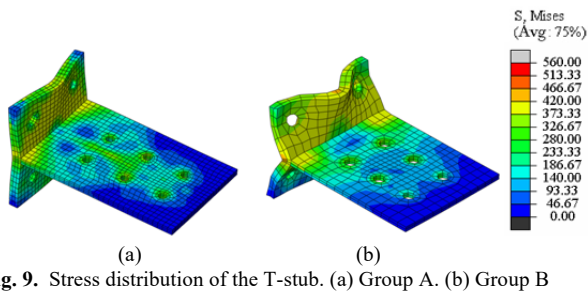
Fig. 9. Stress distribution of the T-stub. (a) Group A. (b) Group B
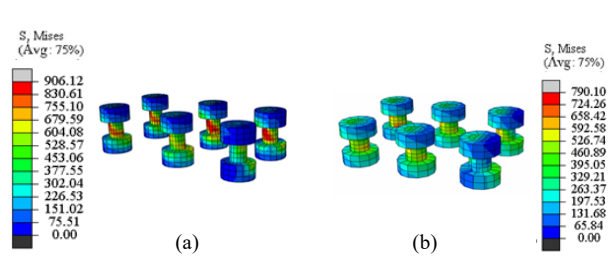
Fig. 11. Stress distribution of the high-strength bolts of the beam flange. (a) Group A. (b) Group B

4.2 Shear transfer path

The moment transfer path and flexural capacity of the joint core area have been widely studied in the literature, but the shear transfer mechanism of the core area of the outer sleeve joint under reciprocating load has not received much research attention. Without direct contact between the beam and column due to the connection of the T-stub, the shear force transmission path and shear force distribution law of different components warrants further study.

Fig. 10. Stress distribution of the high-strength bolts of the column wall. (a) Group A. (b) Group B

By taking the B-HSTJ specimen as an example, the section of the beam–column connection in the joint core area was divided when loaded onto the plastic stage based on FEA as shown in Fig. 12.
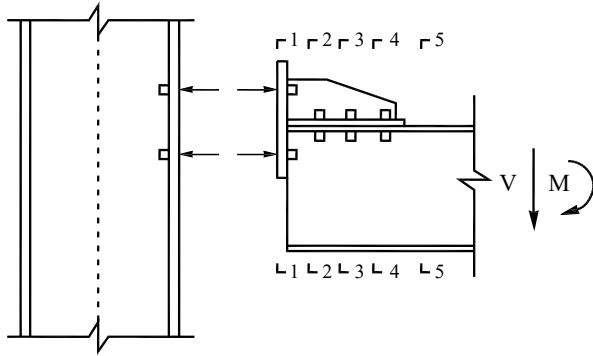
Fig. 12. Sections of the joint core area

A step-by-step calculation was adopted to obtain the shear force distribution of each section. The results are shown in Table 2.

Table 2. Shear force distribution of each section of the joint core area

Components	Shear value of each section (kN)				
	1-1	2-2	3-3	4-4	5-5
High-strength bolts of column wall	118.9				
T-stub flange	43.6				
Stiffener rib		96.2	84.34	42.59	
T-stub web		51.7	58.83	39.98	
Beam web		14.6	19.34	79.95	147.89

According to the shear force distribution of the sections, the shear force transfer mechanism in the core area of the outer sleeve joint can be determined. Specifically, when the vertical shear force of the H-shaped steel beam is transmitted to the beam end section, part of the shear force borne by the beam web is distributed to the T-stub web and stiffener ribs, of which the stiffener ribs bear 26.2% to 59.2% of the shear in the shear force transmission process of the joint core area. The distance from the joint core area decreases, and then the shear force borne by the beam web is reduced. Therefore, the stiffener ribs become the main component of shear resistance. The shear force assumed by the T-stub web accounts for 24.6% to 36.2% of the total shear force of the sections, and its shear action cannot be ignored. In this case, simplifying the T-stub web into a separate tension member in the conventional calculation is unreasonable. At the later stage of loading, relative slippage occurs between the T-stub flange and the outer sleeve, and the shear force is mainly transmitted to the square steel tube column through the high-strength bolts.

4.3 Parameter analysis
The internal force of the outer sleeve joints is complex under the action of the vertical load at the top of the column and the reciprocating load at the beam end. Using the FEA method, the failure modes of the joints under different parameters and the moment–rotation relationships were analyzed to determine the main parameters that affect the seismic performance of the joints, which provide a theoretical basis for the design of the outer sleeve joints.

The analysis parameters were divided into three categories, namely, material parameters, geometric parameters, and load parameters.
(1) Material parameters
Yield strength of the H-shaped steel beam ($f_{y,b}$): $f_{y,b}$=235, 345, 390, 420 (N/mm^2);
Yield strength of the square steel tube column ($f_{y,c}$): $f_{y,c}$=235, 345, 390, 420 (N/mm^2);
Compressive strength of concrete in the square steel tubular column (f_{cu}): $f_{y,c}$=235, 345, 390, 420 (N/mm^2);
(2) Geometric parameters
Beam-to-column linear stiffness ratio ($k_i = \dfrac{E_b I_b H}{E_c I_c L}$):

k_i=0.268, 0.402, 0.447, 0.536, 0.670, 0.804 (of which $E_b I_b$ and $E_c I_c$ are the bending stiffness of the steel beam and square steel tube column, respectively, H is the column height, and L is the length of the steel beam).
Beam-to-column flexural capacity ratio ($k_m = \dfrac{\sum M_b}{\sum M_c}$):

k_m=0.287, 0.346, 0.372, 0.421, 0.476, 0.512, 0.618 ($\sum M_b$ is the sum of the flexural bearing capacity of the beam section under the action of positive and negative bending moments, and $\sum M_c$ is the sum of the flexural bearing capacity of the upper and lower sections of the column).
(3) Load parameters
Axial compression ratio (n): n= 0.2, 0.3, 0.5, 0.7.
During the parameter analysis of the outer sleeve joint, the group A joints were selected as the standard specimens in the experiment. The material strength of steel is Q345, the axial compression ratio is 0.3, and the length of the square steel tube column is 3000 mm.

4.3.1 Yield strength of the H-shaped steel beam $f_{y,b}$

As shown in Fig. 13, when $f_{y,b}$ increases from 235 N/mm^2 to 420 N/mm^2, the failure mode of the specimens is the beam flange buckling failure, thereby indicating that increasing $f_{y,b}$ does not change the original failure mode of the joints. In Fig. 14, $f_{y,b}$ does not affect the initial stiffness of the joints. When $f_{y,b}$ increases from 235 N/mm^2 to 345 N/mm^2, the flexural bearing capacity increases by 20.4%, and the ultimate rotation angle decreases by 8%. As the yield strength of the steel beam continues to increase, the joint bearing capacity does not increase significantly, whereas the hysteretic curve gradually shrinks.
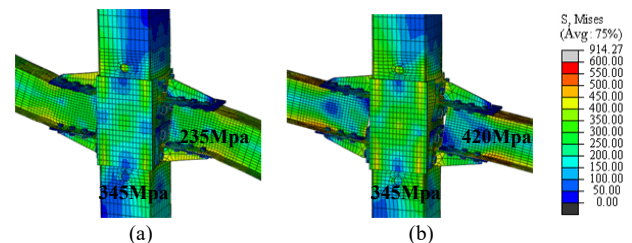
Fig. 13. Influence of the yield strength of the H-shaped steel beam on the failure modes of A-HSTJ specimens. (a) 235Mpa. (b) 420Mpa

4.3.2 Yield strength of the square steel tube column $f_{y,c}$

As shown in Fig. 15, when $f_{y,c}$ increases from 235 N/mm^2 to 420 N/mm^2, the failure of the joint changes from the yield of the column wall to the plastic hinge failure of the

beam flange, indicating that $f_{y,c}$ can affect the failure mode of the joints. Fig. 16 shows that the initial stiffness of the joints is not affected by $f_{y,c}$. Upon entering the yield stage, the increase in the bearing capacity of each joint shows a slight difference. When $f_{y,c}$ increases from $235\ N/mm^2$ to $345\ N/mm^2$, the hysteresis curve quickly converges, and the ductility decreases.

(a)

(b)
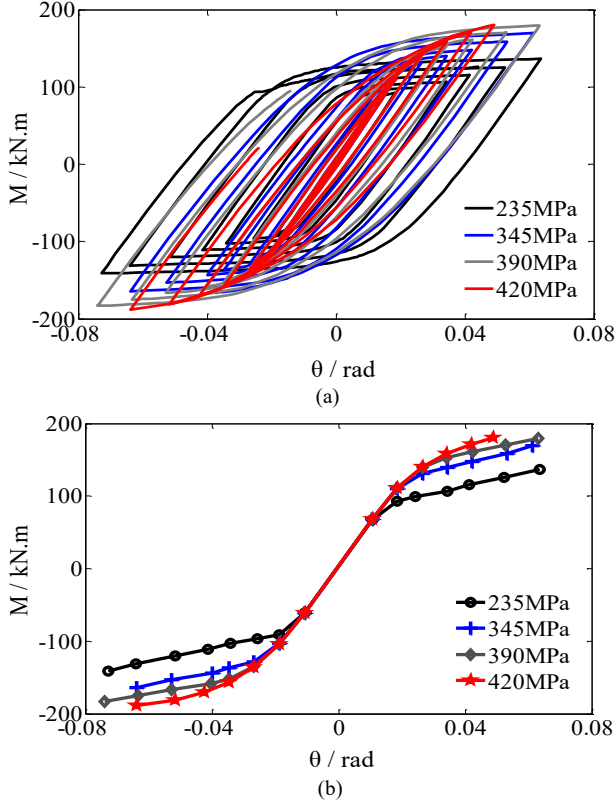
Fig. 14. Influence of the yield strength of the H-shaped steel beam on the moment–rotation curves of A-HSTJ specimens. (a) Moment-rotation hysteresis curves. (b) Moment-rotation skeleton curves

(a)   (b)
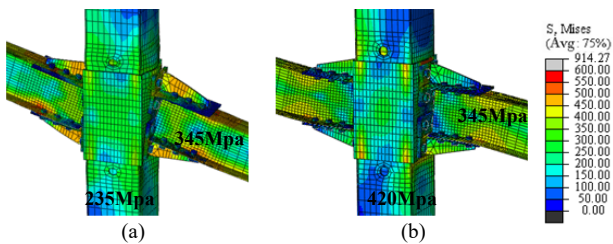
Fig. 15. Influence of the yield strength of the square steel tube column on the failure modes of A-HSTJ specimens. (a) 235Mpa. (b) 420Mpa

(a)

(b)
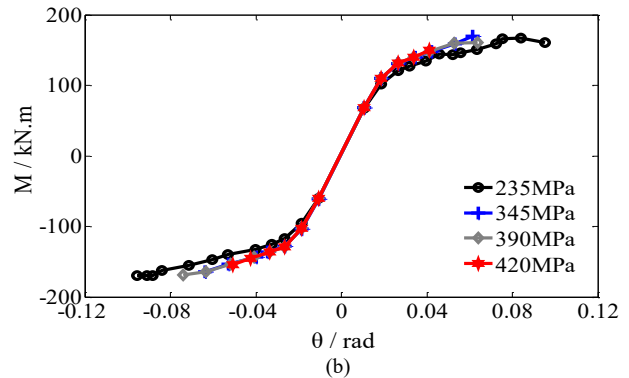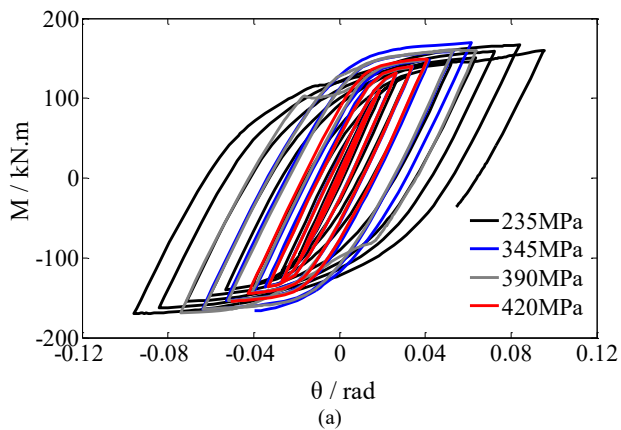
Fig. 16. Influence of the yield strength of the square steel tube column on the moment–rotation curves of A-HSTJ specimens. (b) Moment-rotation skeleton curves

4.3.3 Compressive strength of concrete f_{cu}

As shown in Fig. 17, the concrete effectively constrains the column wall and strengthens the joint area. Increasing f_{cu} does not change the failure mode of the joints, and the specimens form plastic hinges at the beam end. As shown in Fig. 18, increasing f_{cu} only has a slight impact on the bearing capacity and energy consumption of the joints. Although increasing f_{cu} will enhance the modulus of elasticity, the initial bending stiffness of the joint does not increase significantly.

(a)   (b)
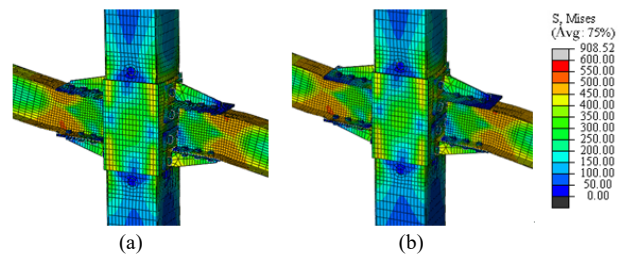
Fig. 17. Influence of the compressive strength of concrete on the failure modes of A-CFSTJ specimens. (a) C30. (b) C80

(a)

(b)
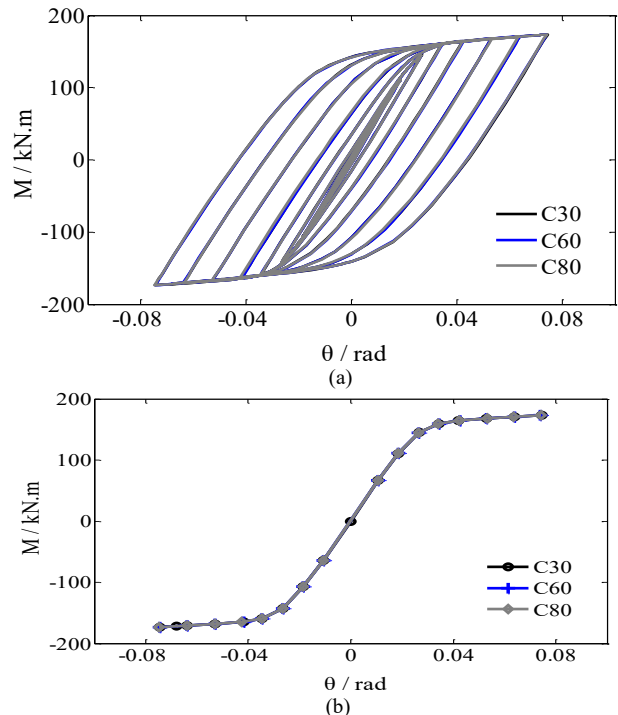
Fig. 18. Influence of the compressive strength of the concrete on the moment–rotation curves of A-CFSTJ specimens. (a) Moment-rotation hysteresis curves. (b) Moment-rotation skeleton curves

4.3.4 Beam-to-column linear stiffness ratio k_i

Both the beam–column section size and member length can change the beam-to-column linear stiffness ratio k_i. In this study, the change in k_i was realized by adjusting the length of the H-shaped steel beam. For specimen A-HSTJ, by taking L as 1000, 1200, 1500, 1800, 2000, 2500 and 3000 mm, parameter k_i varied between 0.268 and 0.804.
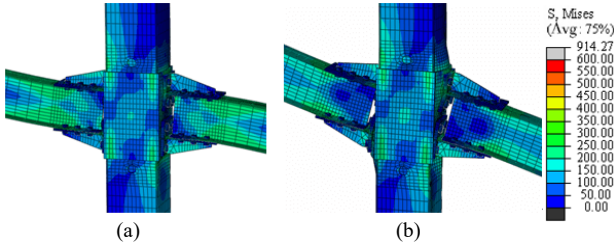
Fig. 19. Influence of beam-to-column linear stiffness ratio on the failure modes of A-HSTJ specimens. (a) $k_i = 0.402$. (b) $k_i = 0.670$

As shown in Fig. 19, the A-HSTJ specimens are dominated by beam flange deformation. As k_i increases, the specimen gradually changes from beam flange buckling failure to joint core failure. Therefore, k_i has a great influence on the failure form of the joints. In this study, when k_i is greater than 0.268 and less than 0.536, the beam flange of the joint yields. The T-stub in the core area of the joint is damaged under tension when k_i is greater than 0.670.

Fig. 20 shows the effect of k_i on the moment–rotation curves of A-HSTJ specimens. When k_i increases from 0.268 to 0.402, the initial stiffness of the joint increases by 25%, but its bearing capacity only increases by 2.9%. Meanwhile, when k_i increases from 0.402 to 0.536, the bearing capacity and initial stiffness of the joint are almost unchanged, whereas its ultimate rotation angle increases by 33.9%. With an increasing k_i, the mechanical parameters of the joint remain the same, but the stress gradually concentrates on the core area of the joint. According to the comprehensive results, the critical value of k_i is set to 0.536.
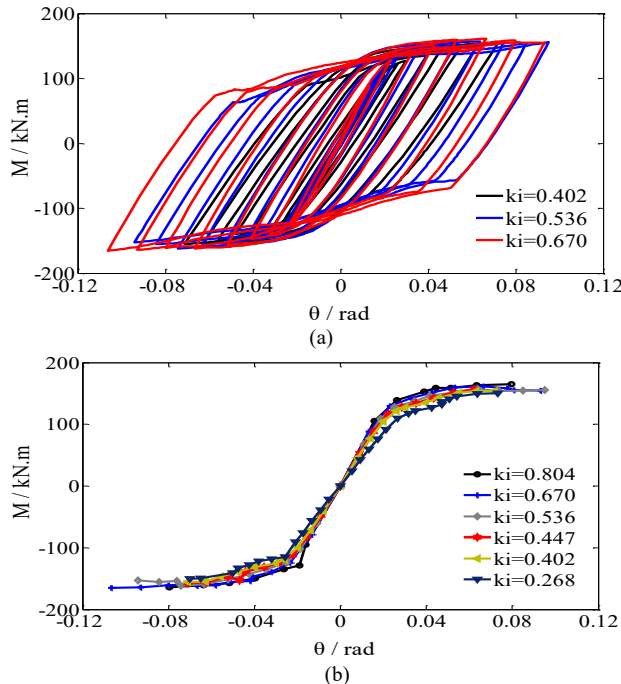
Fig. 20. Influence of beam-to-column linear stiffness ratio on the moment–rotation curves of A-HSTJ specimens. (a) Moment-rotation hysteresis curves. (b) Moment-rotation skeleton curves

4.3.5 Beam-to-column flexural capacity ratio k_m

The beam-to-column flexural capacity ratio k_m is related to $f_{y,b}$, $f_{y,c}$, and section size. However, changing the section size of the beam and column also changes k_m. Therefore, the influence of k_m on the seismic performance of the joint was analyzed by changing the yield strength of the beam and column. After calculation, the k_m values of A-HSTJ specimens were 0.287, 0.346, 0.372, 0.421, 0.476, 0.512, and 0.618, respectively. Fig. 21 shows the failure modes of the specimens under different k_m values.
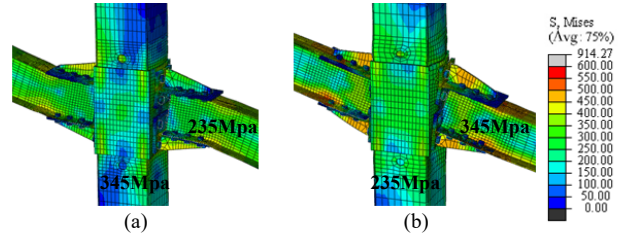
Fig. 21. Influence of beam-to-column flexural capacity ratio on the failure modes of A-HSTJ specimens. (a) $k_m = 0.287$. (b) $k_m = 0.618$

According to the failure modes of the joints, with an increasing k_m, the failure of the joints changes from the buckling of the beam flange to the failure of the T-stub web in the core area. Therefore, k_m greatly affects the failure modes of the joints. When k_m is greater than 0.287 and less than 0.512, the beam end buckles and fails. When k_m is greater than 0.618, the T-stub in the core area is damaged under tension.
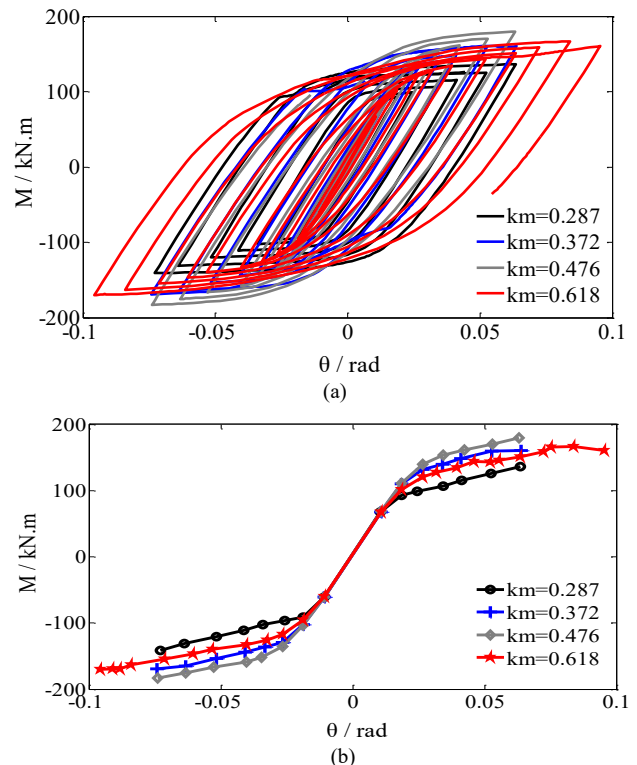
Fig. 22. Influence of beam-to-column flexural capacity ratio on the moment–rotation curves of A-HSTJ specimens. (a) Moment-rotation hysteresis curves. (b) Moment-rotation skeleton curves

Fig. 22 shows that k_m greatly affects the bending moment–rotation curves of the joints. When k_m increases from 0.287 to 0.476, the flexural capacity increases by 25.3%, whereas the ultimate rotation angle does not improve.

When k_m increases from 0.476 to 0.618, although the limit rotation angle increases by 28.2%, the joint is damaged due to a serious column wall bulge. When the k_m values are 0.372 and 0.476, the mechanical properties are almost the same, but the failure mode of the former tends to be the plastic hinge failure of the beam end. The comprehensive results show that the critical value of k_m is 0.372.

4.3.6 Axial compression ratio of column *n*

Fig. 23 shows that the axial compression ratio *n* increases from 0.2 to 0.7 and that the internal force and deformation of the specimens gradually develop from the joint core area to the beam flange, thereby indicating that increasing the axial compression ratio can change the internal force distribution of the joint. However, the failure mode of the joint does not change, and all joints form plastic hinges at the beam ends. Fig. 24 shows that increasing the axial compression ratio only slightly affects the stiffness, flexural capacity, and energy consumption of the joints.
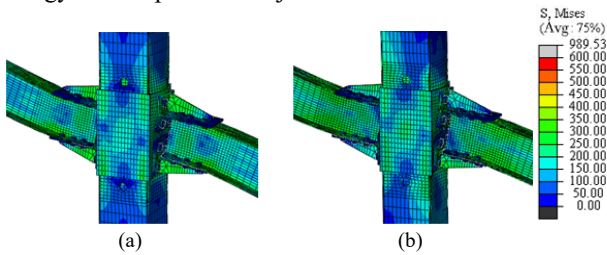
Fig. 23. Influence of axial compression ratio on the failure modes of B-CFSTJ specimens. (a) *n* = 0.2. (b) *n* = 0.7
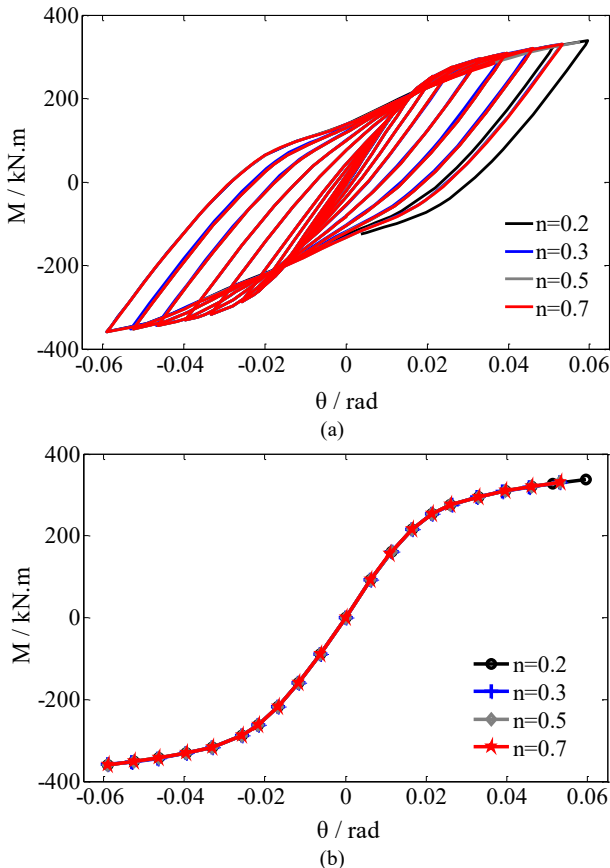
Fig. 24. Influence of axial compression ratio on the moment–rotation curves of B-CFSTJ specimens. (a) Moment-rotation hysteresis curves. (b) Moment-rotation skeleton curves

5. Conclusions

To determine the failure mechanism and seismic influence parameters of the new outer sleeve joints with clear internal force transmission paths and convenient on-site installation, finite element simulations were performed on the outer sleeve joints under low-cycle reciprocating loads. Using the finite element model and parameter analysis, the internal force distribution of each component of the joint was studied, the transmission path of the shear force in the core area of the joint was revealed, and the influence of material parameters, geometric parameters, and load parameters on the failure mode and seismic performance of the joints was discussed. The following conclusions are drawn:

(1) The dimension of the joint has a great influence on the failure mode of the specimens. Plastic hinges appear at the beam ends of the group A specimens, which meet the design requirements of strong joints and weak members. The brittle failure of the T-stub webs of the group B specimens should be avoided as much as possible.

(2) According to the Mises stress diagram, the stress in the core areas of the groups A and B specimens is distributed on the H-shaped steel beam and T-stub, respectively, and corresponds to the failure mode of the tests. The stress on the flanges of the square steel tubular column shows an anti-symmetric distribution, and the stress distribution of the outer sleeves displays the shape of plastic hinge lines.

(3) According to the shear force distribution law in the core area of the joint, the shear force at the beam–column connection is mainly borne by the stiffener ribs. Meanwhile, the shear force transmitted outside of the T-stub web end is borne by the beam web.

(4) The influence of concrete strength and axial compression ratio on the bearing capacity and energy dissipation capacity of the joint is limited. The yield strength of the H-shaped steel beam and square steel tube column has a certain influence on the flexural bearing capacity and failure mode of the joint.

(5) By increasing the linear stiffness ratio and flexural capacity ratio of beam-to-column, the failure mode of the joint changes from the failure of the plastic hinge at the beam end to the failure of the core area of the joint. Comprehensive analysis results show that the recommended linear stiffness ratio and flexural capacity ratio of beam-to-column are 0.536 and 0.372, respectively.

This study comprehensively considers the failure mode, mechanical properties, and stress variation law of outer sleeve joints, which accurately reflect the failure mechanism of the joints in the process of reciprocating loading. Meanwhile, the parameter analysis results provide theoretical guidance for the design values of actual steel structure engineering. However, construction factors cannot be easily considered in finite element modeling, and the refined numerical model warrants further in-depth study.

_____

References

1. Engelhardt, M. D., Husain, A. S., "Cyclic-loading performance of welded flange-bolted web connections". *Journal of Structural Engineering*, 119(12), 1993, pp.3537-3550.
2. Zhu, W. Q., Mo, Z. P., Liu, Y. J., "Tensile performance of concrete filled square steel tube exterior-diaphragm connections stiffened with PBL". *China Civil Engineering Journal*, 53(10), 2020, pp.1-12,35.
3. Wang, M., Bi, P., Li, F. X., "Design of steel frame cover plate connected joints with low yield point steel ductile fuses". *Engineering Mechanics*, 37(2), 2020, pp. 168-182.
4. Cho, B. H., Lee, J. S., Kim, H., Kim, D. J., "Structural performance of a new blind-bolted frame modular beam-column connection under lateral loading". *Applied Sciences*, 9(9), 2019, pp.1929.
5. Yu, H., Li, W., "Comparison of steel frames with RWS and WFP beam-to-column connections through seismic fragility analysis". *Advances in Structural Engineering*, 24(8), 2021, pp. 1583-1598.
6. Liu, M. M., Jiang, H. Y., "Research on seismic behavior of beam-column connections with stiffeners at web openings". *Steel Construction*, 33(11), 2018, pp. 7-15.
7. Loh, H. Y., Uy, B., Bradford, M. A., "The effects of partial shear connection in composite flush end plate joints Part I-experimental study". *Journal of Constructional Steel Research*, 62(4), 2006, pp.378-390.
8. Zhang, D., Tao, Z., Zhang, L., "Experimental and numerical analysis of the seismic behavior of outer shell joints for h-shaped steel beam and square tubular column". *Journal of Engineering Science and Technology Review*, 10(2), 2017, pp. 178-190.
9. Liu, X. C., Cui, F. Y., Zhan, X. X., Yu, C., Jiang, Z. Q., "Seismic performance of bolted connection of H-beam to HSS-column with web end-plate". *Journal of Constructional Steel Research*, 156, 2019, pp. 167-181.
10. Wang, P., Wang, Z., Pan, J., Zheng, Y., Liu, D., "Cyclic behavior of steel beam to CFT column connections with gusset plates". *Advances in Civil Engineering*, 2019,2019, pp.3798671.
11. Roudsari, M. T., Sohaei, S., Torkaman, M., Safaee, S. A., Tahmasebi, S., Mohammadi, S., Ghiasvand, M. M., "Presenting a new detail for the rigid connection between I-shaped beam and concrete-filled steel tube column with stiffened channel link". *International Journal of Steel Structures*, 20(2), 2020, pp. 655-667.
12. Zhang, A. L., Su, L., Jiang, Z. Q., Kang, Y. T., Qiu, P., "Cyclic loading tests of earthquake-resilient prefabricated steel cross joints with different FCP connections". *Structures*, 32, 2021, pp. 1-14.
13. Zhan, X. X., Liu, X. C., Feng, S., Yu, C., "Seismic performance of a square HSS column to H-section beam bolted connection with double cover plate". *Engineering Structures*, 231, 2021, pp.111729.
14. Heidari, P. S., Aziminejad, A., Moghadam, A. S., Jafari, M. A., "Evaluation of drilled flange connections with combined arrangements of holes and notches". *Bulletin of Earthquake Engineering*, 18(14), 2020, pp. 6487-6532.
15. Parvari, A., Zahrai, S. M., Mirhosseini, S. M., Zeighami, E., "Numerical and experimental study on the behavior of drilled flange steel beam to CFT column connections". *Structures*, 28, 2020, pp. 726-740.
16. Vajdian, M., Zahraei, S. M., Mirhosseini, S. M., Zeighami, E., "Investigation of seismic performance of (RBS) and drilled flange connection (DFC) containing rhombus shaped hole in steel moment frames". *Australian Journal of Civil Engineering*, 18(2), 2020, pp. 246-262.
17. Roudsari, M. T., Abdollahi, F., Salimi, H., Azizi, S., Khosravi, A. R., "The effect of stiffener on behavior of reduced beam section connections in steel moment-resisting frames". *International Journal of Steel Structures*, 15(4), 2015, pp. 827-834.
18. Kolbadi, S. M. S., Piri, H., Keyhani, A., Kolbadi, S. M. S., Mirtaheri, M., "Seismic performance evaluation of slotted-web and bolt-flange plate moment connection". *Earthquakes and Structures*, 20(6), 2021, pp. 655-667.
19. Imanpour, A., Torabian, S., Mirghaderi, S. R., "Seismic design of the double-cell accordion-web reduced beam section connection". *Engineering Structures*, 191, 2019, pp.23-38.
20. Jiang, Z. Q., Yang, X. F., Dou, C., Li, S. H., Zhang, A. L., "Seismic performance of prefabricated corrugated web beam-column joint with replaceable cover plates". *Advances in Structural Engineering*, 22(5), 2019, pp. 1161-1174.
21. Hibbit, H. D., Karlsson, B. I., Sorensen, E. P., "*ABAQUS user's manual Version 6.12*". Pawtucket, USA: Hibbitt, Karlsson & Sorensen Inc, 2012.
22. Yang, L. F., Xie, W. W., Rong, Y., Jiang, L. F., "Constitutive relations and failure criterion for rectangular concrete-filled steel tube members under pure bending". *China Civil Engineering Journal*, 52(1), 2019, pp. 60-70.